Cascaded Active and Passive Quasi-Optical Grids

Wayne A. Shiroma, *Student Member, IEEE,* Scott C. Bundy, *Member, IEEE,*
Stein Hollung, Brenda D. Bauernfeind, and Zoya B. Popovic, *Member, IEEE*

Abstract—**A general method for analyzing systems of cascaded grids is presented. The analysis is based on a full-wave theory for arbitrary periodic metal gratings printed on dielectrics and loaded with active and/or passive lumped devices. Each quasi-optical component is characterized as a multiport network, in which two of the ports represent the free-space regions on the two sides of the grid surface, and the remaining ports are connected to the devices. This approach allows cascading of quasi-optical components using transmission-line theory. Several examples are presented which demonstrate the theory: free-space filters containing lumped capacitors and resistors; an X-band transmission-mode linear-to-circular polarization converter; an S-band voltage-controlled frequency-selective surface; and a C-band mode-selective grid oscillator.**

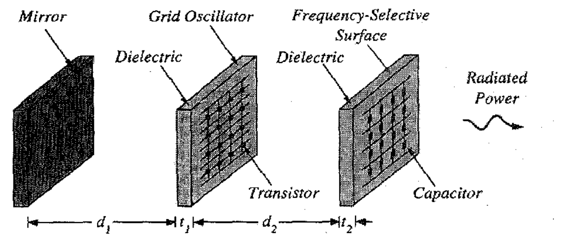

Fig. 1. An example of a simple quasi-optical system consisting of a transistor grid oscillator cascaded with a capacitively loaded frequency-selective surface.

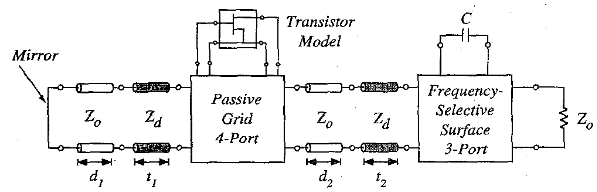

Fig. 2. Equivalent circuit for the quasi-optical system shown in Fig. 1. The passive grid geometry is represented as a four-port network, the frequency-selective surface as a three-port network, the dielectric and free-space regions as TEM-mode transmission lines, and the mirror as a short. The resistor represents the radiation into free space.

I. Introduction

A NUMBER OF ACTIVE quasi-optical grids have been demonstrated in recent years: oscillators [1], amplifiers [2], mixers [3], phase shifters [4], [5], multipliers [6], and switches [7]. In active grids, solid-state devices periodically load a grating printed on a dielectric substrate. In some applications, devices may be loaded on both sides of the dielectric [8]. Two methods based on a unit-cell approach (infinite-grid approximation) have proven useful for designing active grids: an EMF theory (e.g., [1]) and a full-wave theory for grid oscillators [9]. While the EMF method is limited to specific grid geometries where the current distribution can be assumed, the full-wave theory presented in [9] allows arbitrary periodic metal patterns on one or both sides of a dielectric substrate, and characterizes the passive part of the grid as an equivalent multiport network. This passive network is connected to an active device model to form an equivalent circuit for the grid oscillator, which can then be analyzed using a conventional circuit simulator. This technique has been successfully demonstrated in several grid oscillator designs, but cannot be used for analyzing systems consisting of multiple quasi-optical components, such as the one shown in Fig. 1.

In [10], we presented an approach in which each planar structure in a cascaded system is characterized separately using the full-wave analysis. All of the equivalent networks are then cascaded in a transmission-line circuit, such as the one shown in Fig. 2. Using this building-block approach, an entire system composed of an arbitrary number of active and/or passive grids can be analyzed. Design iterations are fast, since changes in the dielectric constant or thickness are implemented by changing transmission-line characteristics.

In this paper, we present several cascaded grid systems illustrating this design approach: free-space filters containing lumped capacitors and resistors; an X-band transmission-mode linear-to-circular polarization converter; an S-band voltage-controlled frequency-selective surface; and a C-band mode-selective grid oscillator.

II. Method of Approach

For the multiport characterization of passive grid geometries presented in [9], the only accessible ports are those to which the active device is connected. In this work, we generalize the model by introducing two additional ports which represent the free-space regions in front and in back of the grid. These two ports are equivalent TEM waveguides representing the unit-

Manuscript received March 1, 1995; revised July 10, 1995. This work was supported in part by the U.S. Army Research Office Contract #DAAL03-92-G-0265 and the AASERT Program, and in part by the National Science Foundation under a Presidential Faculty Fellow Award and the Research Experience for Undergraduates Program.

W. A. Shiroma, S. Hollung, B. D. Bauernfeind, and Z. B. Popovic are with the Department of Electrical and Computer Engineering, University of Colorado, Boulder, CO 80309 USA.

S. C. Bundy is with Superconducting Core Technologies, Golden, CO 80401 USA.

IEEE Log Number 9415463.

0018–9480/95$04.00 © 1995 IEEE

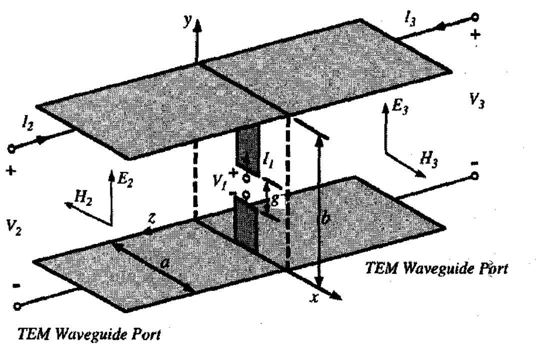

Fig. 3. The parallel-plate waveguide corresponding to a unit cell of width a and height b. The solid lines represent the horizontal electric walls and the dashed lines represent the vertical magnetic walls. This waveguide supports a TEM wave with a y-directed electric field and an x-directed magnetic field. When the unit cell at $z = 0$ is driven with a source, plane waves travel away from the structure in both the $+z$ and $-z$ directions.

cell boundary conditions, as shown in Fig. 3. To characterize the grid as an equivalent multiport network, we define wave variables at each port

$$a_n = \frac{1}{2}\left(\frac{V_n}{\sqrt{Z_{on}}} + I_n\sqrt{Z_{on}}\right) \quad \text{and}$$
$$b_n = \frac{1}{2}\left(\frac{V_n}{\sqrt{Z_{on}}} - I_n\sqrt{Z_{on}}\right)$$

where $Z_{on} = \eta_o b/a$ is the characteristic impedance of the unit-cell waveguide. At the device ports, the voltages and currents are found as in [9], where $V = -E_g g$ is the voltage in a gap of width g and I is determined from the moment method. At the waveguide ports, the voltages and currents are defined in terms of the electric field E_o and magnetic field $H_o = \pm E_o/\eta_o$ for a TEM wave in the waveguide. The voltage across the waveguide plates is $V = -E_o b$ and the current is $I = E_o a/\eta_o$, giving $a_n = 0$ and $b_n = -E_o\sqrt{ab/\eta_o}$ for a wave propagating away from the grid.

Scattering parameters can be derived once the wave variables are found, but the details are slightly different depending on the number of device ports in the unit cell. Therefore, let us consider three separate cases.

The simplest case is that of a passive grating with no device ports, such as a free-space filter. For this structure, a two-port characterization is required, where both ports are unit-cell waveguide ports. The free-space reflection coefficient Γ_{fs} is found by exciting one of these ports with a plane wave, as in [9]. The S-parameters are then given by $S_{11} = \Gamma_{fs}$ and $S_{21} = \Gamma_{fs} + 1$, where the subscripts 1 and 2 represent the waveguide ports. Since both waveguides are identical, $S_{22} = S_{11}$ and $S_{12} = S_{21}$.

The second case is a structure with one device port in the unit cell, as in a diode-loaded grid. Let port 1 represent the device port and ports 2 and 3 represent the waveguide ports. With the waveguides terminated in their characteristic impedance $\eta_o b/a$, port 1 is driven with a voltage source as described in [9]. The moment method is used to calculate the current on the structure, and the resulting radiated electric and magnetic fields are determined. The corresponding wave variables are then used to compute S_{11}, S_{21}, and S_{31}. By reciprocity, $S_{12} = S_{21}$ and $S_{13} = S_{31}$. To determine the four remaining S-parameters, the free-space reflection coefficient Γ_{fs} is computed by shorting the device port and driving one of the waveguides with an incident plane wave. In this case, since $a_1 = -b_1$ and $a_3 = 0$, the S-parameter equations can be written as

$$\frac{b_2}{a_2} = S_{22} - \frac{S_{12}S_{21}}{1 + S_{11}} = \Gamma_{fs} \quad \text{and}$$
$$\frac{b_3}{a_2} = S_{32} - \frac{S_{12}S_{31}}{1 + S_{11}} = \Gamma_{fs} + 1$$

which can be solved for S_{22} and S_{32}. Since both waveguides are identical, $S_{33} = S_{22}$ and $S_{23} = S_{32}$.

All of the S-parameters found above are normalized to the TEM waveguide impedance $\eta_o b/a$. To provide compatibility with circuit simulators, the S-parameters are renormalized to 50 Ω. The procedure for finding the S-parameters of a structure with two device ports is similar to the other two cases described above; details of the derivation can be found in [11].

The analysis above characterizes the grid metallization alone without including the effect of the dielectric substrate. The dielectric is modeled as a TEM-mode transmission line connected to the multiport network, as shown in Fig. 2. However, this equivalent circuit neglects the added capacitance in the gap due to the dielectric. To compensate for this, a small lumped capacitor (a few fF) is placed across the device ports of the multiport network. The capacitance value can be electrostatically estimated from the geometry of the structure.

The method described here may be applied to any cascade connection of quasi-optical components, provided that the grids are spaced far enough apart so that only TEM coupling takes place. In this implementation of the analysis, it is assumed that the dimensions of the unit cell and the frequency of operation are such that the higher-order modes are cut off in the unit-cell waveguide. The spacing between grids is then limited by the distance over which these evanescent modes have sufficiently decayed. For example, in [9] the total electric field within a single unit cell was computed at several distances from the plane of the structure. It is seen that the higher-order modes become negligible within a small fraction of a fundamental-mode guided wavelength. For most practical grid spacings, the assumption of strictly TEM-mode coupling is satisfied. However, this is not a fundamental limitation of the analysis used here since the theory can be generalized to include the coupling effects due to higher-order modes by including an additional port and transmission line for each mode.

III. Experimental Results

Several quasi-optical components are presented in this section. The specific design procedure depends on the type of component desired. For illustration purposes, we summarize the design approach for a component consisting of a single planar structure with unit cells having a single device port. First, a nominal metal grid pattern is selected. This structure is characterized by a multiport network as described in the

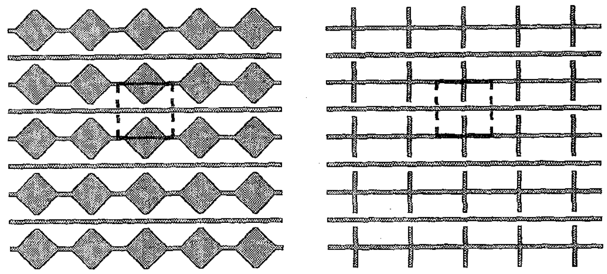

(a) (b)

Fig. 4. Two different grid patterns, (a) one with bowtie radiating elements and (b) another with dipole radiating elements. Each unit cell is 15 mm by 15 mm and contains two ports to which lumped devices may be connected. The grids are printed on 0.5-mm-thick *Duroid* substrates with $\varepsilon_r = 2.2$.

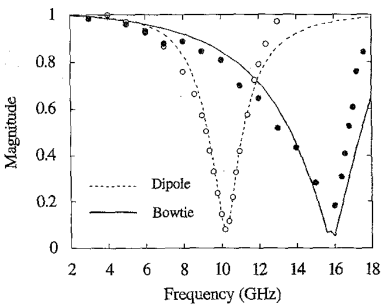

(a)

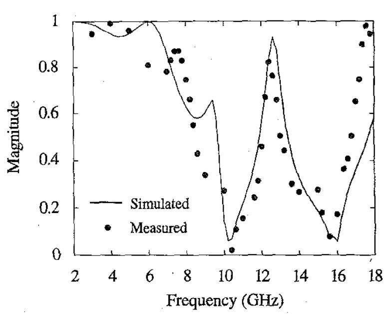

(b)

Fig. 5. Magnitude of the transmission coefficient of (a) each grid alone, and (b) the cascaded grids separated by 35 mm. The lines represent the theory and the dots represent the measured data.

previous section. Then, transmission lines representing the dielectric and air regions, as well as an appropriate model for the one-port device, are connected to the multiport network and the resulting circuit is analyzed on a circuit simulator. Within the simulator, either the transmission-line parameters can be adjusted or another lumped device can be used to optimize the system performance. The overall circuit can be further improved by varying one or more dimensions of the unit cell and reanalyzing the structure. This procedure is iterated until a system with the desired operating characteristics is obtained.

To validate the theory, several systems of cascaded grids were fabricated and measured. Each grid contains ports which may be loaded with active or passive devices. All of the

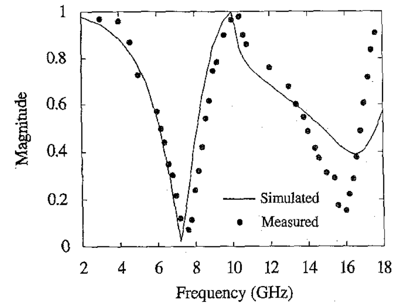

(a)

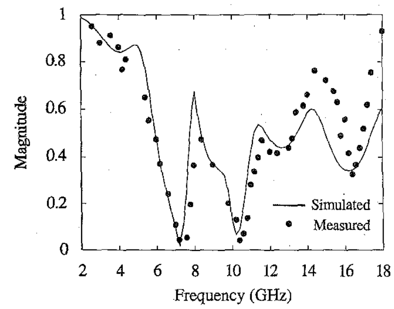

(b)

Fig. 6. Magnitude of the transmission coefficient of (a) the bowtie grid loaded with a 0.5-pF capacitor in each unit cell, and (b) the capacitively loaded bowtie grid cascaded with the unloaded dipole grid 40 mm away.

components described below operate in transmission mode and can easily be cascaded into systems.

A. Free-Space Filters Containing Lumped Elements

Fig. 4 shows two examples of free-space filters. Simulations and measurements of the transmission coefficient of the unloaded grids are shown in Fig. 5. The bowtie and dipole grids exhibit resonances at 15.8 and 10.2 GHz, respectively. When these grids are cascaded, the individual resonances of each grid are observed, as shown in Fig. 5(b). If the bowtie grid is loaded with a 0.5-pF capacitor in each unit cell, the resonance shifts from 15.8 to 7.2 GHz, as shown in Fig. 6(a). Fig. 6(b) illustrates the effect of cascading the capacitively loaded bowtie grid with the unloaded dipole grid. Once again, the resonances due to the individual grids are seen in the response of the cascaded system. When each unit cell of the bowtie grid is loaded with an additional 100-Ω resistor in the second port, the resulting characteristic shown in Fig. 7 is obtained. As expected, the resistor introduces loss and reduces the Q of the grating.

B. Linear-to-Circular Polarization Converter

Several types of circular polarizers have been recently reported (e.g., [12], [13]). Here, we present a transmission-mode linear-to-circular polarization converter consisting of capacitively loaded dipole grids, as shown in Fig. 8. Each grid contains an array of dipoles oriented 45° with respect to a vertically polarized incident plane wave. The field com-

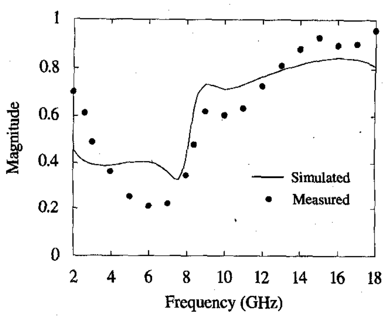

Fig. 7. Magnitude of the transmission coefficient of the bowtie grid loaded with a 0.5-pF capacitor and a 100-Ω resistor in each unit cell.

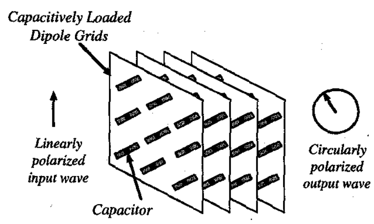

Fig. 8. A transmission-mode linear-to-circular polarization converter. Four capacitively loaded dipole grids are cascaded to achieve low transmission loss. The grids are printed on 0.5-mm-thick *Duroid* substrates with $\varepsilon_r = 2.2$. Surface-mount capacitors are soldered across the metallization gap.

ponent parallel to the dipoles is phase-shifted 90° relative to the orthogonal component, resulting in a circularly polarized transmitted wave.

For a 10-GHz design, the dipoles are 10 mm long and periodically spaced 13 mm apart. A 100-pF chip capacitor is soldered across each of the 1-mm gaps. To obtain low transmission loss, four identical grids spaced 5.5 mm apart are required.

To compare simulation and measurement, the transmission coefficient was measured with the dipoles oriented parallel to the polarization of the incoming plane wave. The frequency response shown in Fig. 9 shows good agreement with the theory. To determine the axial ratio, the transmission coefficient was measured by rotating a receiving horn in the far field. Fig. 10 shows that the output wave is nearly circularly polarized at 8.4 GHz, where the axial ratio is 1.3 dB and the transmission loss is 1.1 dB. The axial ratio is better than 3 dB over a 8% bandwidth. The best axial ratio was measured at a lower frequency than expected, possibly due to an underestimate in modeling the capacitor lead inductance as well as experimental error in positioning the grids. If both the inductance and spacing are increased, simulations show that the polarizer would operate at a lower frequency.

C. Voltage-Controlled Frequency-Selective Surface

To demonstrate the theory for an array of control devices, a varactor-diode loaded grid was designed to serve as a tunable frequency-selective surface. Varactor diodes (Metelics MSV-34) with a rated $C_{\max}/C_{\min}$ ratio of 4 : 1 were used in this grid. As the reverse voltage increases, the resonant frequency varies from 2.56 GHz at 0 V bias to 3.44 GHz at −20 V bias,

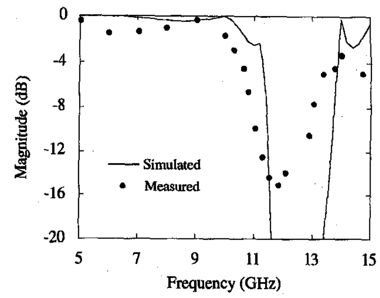

Fig. 9. Simulated and measured transmission coefficient magnitude when the dipoles are oriented parallel to the polarization of the incident plane wave.

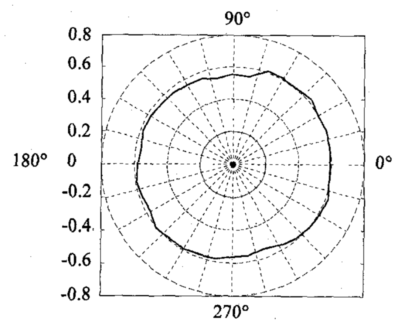

Fig. 10. Magnitude of the transmission coefficient at 8.4 GHz as a function of the rotation angle of the receiving horn antenna. The measurement includes the inherent 3-dB polarization loss of the linearly polarized horn antenna. The ratio of the major to minor axis of the polarization ellipse is the axial ratio.

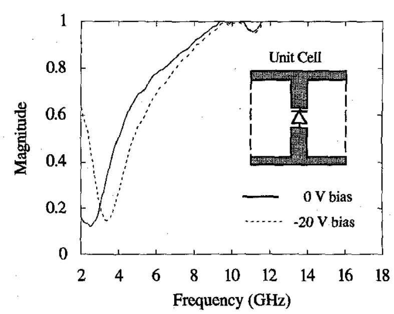

Fig. 11. Magnitude of the transmission coefficient for a varactor-diode loaded grid. The unit cell is 15 mm × 15 mm.

as shown in Fig. 11. Over the entire 30% tuning bandwidth, the transmission level at resonance changes by less than 1%.

D. Mode-Selective Grid Oscillator

A 25-PHEMT grid oscillator was fabricated on 2.54-mm-thick *Duroid* with $\varepsilon_r = 10.5$. The period of the grid is 8 mm with 1-mm-wide bias lines and radiating leads. A mirror is placed directly behind the dielectric substrate.

The grid oscillates at 4.6 GHz with an effective radiated power (ERP) of 0.07 W. The cross-polarization ratio is 11 dB and the second harmonic is −9 dBc. When additional dielectric layers (*Stycast HiK* with $\varepsilon_r = 10$) are inserted between the substrate and mirror, the oscillator unlocks as

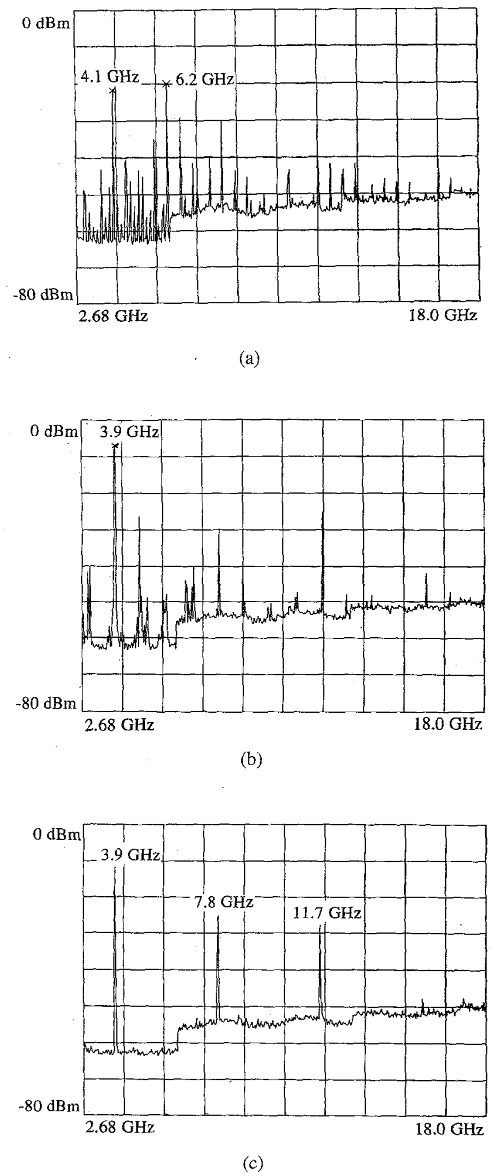

Fig. 12. Spectrum of (a) the unlocked grid oscillator with two competing modes at 4.1 and 6.2 GHz; (b) the grid oscillator with a partially reflecting front mirror; and (c) the locked oscillator cascaded with a voltage-controlled frequency-selective surface biased at -4 V. The power levels shown represent the power received by a low-gain horn antenna in the far field.

shown in Fig. 12(a). This plot shows competing oscillation modes at 4.1 and 6.2 GHz. By adjusting the gate bias, the oscillator locks at 6.2 GHz with an ERP of 0.25 W, cross-polarization of 14 dB, and second harmonic level of -28 dBc.

Since the transistor has saturated gain over a broad frequency range, in principle a number of locked modes could be obtained. However, the oscillator could not lock to the 4-GHz mode through bias tuning or front-mirror tuning alone. The closest we came to achieving a lock at 4 GHz is shown in Fig. 12(b), where a 2.54-mm-thick slab of $\varepsilon_r = 10.5$ *Duroid* was used as a partially reflecting mirror placed in front of the grid. This mirror provided 46% reflectivity at 3.9 GHz and 63% at 6.2 GHz.

By using a frequency-selective front mirror, such as the one described in Part C, the build-up of a particular oscillation mode could be enhanced. By providing a higher cavity Q for the desired mode, while simultaneously lowering the Q for the unwanted mode, the grid oscillator would injection-lock to the higher-Q mode alone. Controlling the cavity Q could be achieved by varying the bias across the diode. Unlike the varactor grid used in [8], this diode grid is not used as a frequency tuner, but rather as a variable-reflectance surface.

Replacing the front mirror slab with the voltage-controlled frequency-selective surface, the spectrum shown in Fig. 12(c) is obtained. At -4 V, this surface presents reflectivities of 85 and 42% at 3.9 and 6.2 GHz, respectively. The oscillator locks at 3.9 GHz with an ERP of 0.26 W, a cross-polarization of 12 dB, and a second harmonic level of -13 dBc.

The two oscillation modes are truly competitive, since they both have about the same power. In short, the multimoded grid oscillator can operate in a single mode by electronically varying the cavity Q to enhance the desired mode.

IV. Conclusion

The method described in this paper is useful for analyzing cascaded quasi-optical grids loaded with active and/or passive devices. Several experimental components are presented. Free-space filters demonstrate tuning between 2 and 18 GHz when different geometries with the same period are loaded with lumped capacitors. An X-band linear-to-circular polarization converter with 1.1 dB transmission loss demonstrates an axial ratio of 1.3 dB. By cascading a 25-PHEMT C-band grid oscillator with a 30%-bandwidth voltage-controlled frequency-selective surface, mode selection is possible. Using the approach presented here, a system consisting of an arbitrary number of cascaded active and passive grids can be analyzed.

References

[1] Z. B. Popovic, R. M. Weikle II, M. Kim, and D. B. Rutledge, "A 100-MESFET planar grid oscillator," *IEEE Trans. Microwave Theory Tech.*, vol. 39, pp. 193–200, Feb. 1991.

[2] M. Kim, E. A. Sovero, J. B. Hacker, M. P. De Lisio, J.-C. Chiao, S.-J. Li, D. R. Gagnon, J. J. Rosenberg, and D. B. Rutledge, "A 100-element HBT grid amplifier," *IEEE Trans. Microwave Theory Tech.*, vol. 41, pp. 1762–1771, Oct. 1993.

[3] J. B. Hacker, R. M. Weikle II, M. Kim, M. P. De Lisio, and D. B. Rutledge, "A 100-element planar Schottky diode grid mixer," *IEEE Trans. Microwave Theory Tech.*, vol. 40, pp. 557–562, Mar. 1992.

[4] W. W. Lam, C. F. Jou, H. Z. Chen, K. S. Stolt, N. C. Luhmann Jr., and D. B. Rutledge, "Millimeter-wave diode-grid phase shifters," *IEEE Trans. Microwave Theory Tech.*, vol. 36, pp. 902–907, May 1988.

[5] L. B. Sjogren, H.-X. Liu, X. Qin, C. W. Domier, and N. C. Luhmann Jr., "Phased-array operation of a diode grid impedance surface," *IEEE Trans. Microwave Theory Tech.*, vol. 42, pp. 565–572, Apr. 1994.

[6] C. F. Jou, W. W. Lam, H. Z. Chen, K. S. Stolt, N. C. Luhmann Jr., and D. B. Rutledge, "Millimeter-wave diode-grid frequency doubler," *IEEE Trans. Microwave Theory Tech.*, vol. 36, pp. 1507–1514, Nov. 1988.

[7] K. D. Stephan and P. F. Goldsmith, "W-band quasioptical integrated PIN diode switch," in *1992 IEEE MTT-S Int. Microwave Symp. Dig.*, Albuquerque, NM, pp. 591–594.

[8] T. B. Mader, S. C. Bundy, and Z. B. Popovic, "Quasi-optical VCOs," *IEEE Trans. Microwave Theory Tech.*, vol. 41, pp. 1775–1781, Oct. 1993.

[9] S. C. Bundy and Z. B. Popovic, "A generalized analysis for grid oscillator design," *IEEE Trans. Microwave Theory Tech.*, vol. 42, pp. 2486–2491, Dec. 1994.
[10] S. C. Bundy, W. A. Shiroma, and Z. B. Popovic, "Analysis of cascaded quasi-optical grids," in *1995 IEEE MTT-S Int. Microwave Symp. Dig.*, Orlando, FL, pp. 601–604.
[11] S. C. Bundy, *Analysis and Design of Grid Oscillators*, Ph.D. dissertation, Univ. of Colorado, Boulder, Dec. 1994.
[12] T.-K. Wu, "Meander-line polarizer for arbitrary rotation of linear polarization," *IEEE Microwave and Guided Wave Lett.*, vol. 4, pp. 199–201, June 1994.
[13] A. D. Shatrow, A. D. Chuprin, and A. N. Sivov, "Constructing the phase converters consisting of arbitrary number of translucent surfaces," *IEEE Trans. Antennas Propagat.*, vol. 43, pp. 109–113, Jan. 1995.

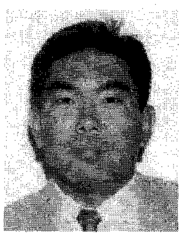

Wayne A. Shiroma (S'85) was born in Los Angeles, CA on February 4, 1963. He received the B.S. degree in electrical engineering from the University of Hawaii at Manoa in 1986 and the M.Eng. degree in electrical engineering from Cornell University, Ithaca, NY, in 1987. He is currently working toward the Ph.D. degree in electrical engineering at the University of Colorado at Boulder.

He served as a Member of the Technical Staff at Hughes Aircraft Company, El Segundo, CA, developing solid-state power amplifiers for satellite communications. His research interests include microwave, millimeter-wave, and quasi-optical circuits.

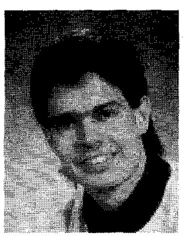

Scott C. Bundy (S'92-M'95) was born on November 15, 1966, in Denver, CO. He received the B.S., M.S., and Ph.D. degrees in electrical engineering at the University of Colorado at Boulder in 1990, 1992, and 1994, respectively.

In 1995, he joined Superconducting Core Technologies, in Golden, Colorado, where he works in product development as a member of the technical staff. His research interests include quasi-optical oscillators, moment method analysis of periodic grid structures, and superconducting applications of microwave circuits.

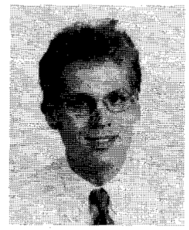

Stein Hollung was born in Oslo, Norway, on March 7, 1970. He graduated from Oslo College of Engineering with an electrical engineering degree in 1992, and received the B.S. and M.S. degrees in electrical engineering from the University of Colorado at Boulder in 1994 and 1995, respectively. He is currently working towards a Ph.D. degree in electrical engineering at the same university.

Brenda D. Bauernfeind was born in El Paso, TX on April 26, 1973. She is currently pursuing the B.S. degree in electrical engineering at the University of Colorado at Boulder.

Zoya Basta Popovic (S'86-M'90) was born in Belgrade, Yugoslavia, in 1962. She received the Dipl.Ing. degree from the University of Belgrade, Serbia, Yugoslavia and the M.S. and Ph.D. degrees from the California Institute of Technology, Pasadena, in 1985, 1986, and 1990, respectively.

In 1990, she joined the University of Colorado, Boulder, where she is now an Associate Professor in Electrical Engineering. Her research interests include microwave and millimeter-wave quasi-optical techniques, microwave and millimeter-wave active antennas and circuits, and electromagnetic modeling of antennas and circuits.

Dr. Popovic received the IEEE MTT 1993 Microwave Prize. Also in 1993, she received the URSI Young Scientist Award and the National Science Foundation Presidential Faculty Fellow Award.